Northumbria Research Link

www.northumbria.ac.uk/nrl

northumbria
UNIVERSITY NEWCASTLE

The Physics of H-Darrieus Turbine Starting Behaviour

Supakit Worasinchai
National Metal and Materials
Technology Center (MTEC)
Renewable Energy Laboratory
Pathum Thani, Thailand
Email: supakitw@mtec.or.th

Grant L. Ingram *
University of Durham
School of Engineering
and Computing Sciences
South Road, Durham, UK
Email: g.l.ingram@durham.ac.uk

Robert G. Dominy
Northumbria University
Faculty of Engineering and Environment
Newcastle upon Tyne, UK
Email: robert.dominy@northumbria.ac.uk

ABSTRACT

This paper provides a resolution to the contradictory accounts of whether or not the Darrieus turbine can self-start. The paper builds on previous work proposing an analogy between the aerofoil in Darrieus motion and flapping-wing flow mechanisms. This analogy suggests that unsteadiness could be exploited to generate additional thrust and that this unsteady thrust generation is governed by rotor geometry. Rotors which do not exploit this unsteadiness will not self-start.

To confirm the hypothesis, unsteady effects were measured and then incorporated into a time-stepping rotor analysis and compared to experimental data for self-starting wind turbines. When unsteady effects were included the model was able to predict the correct starting behaviour.

The fundamental physics of starting were also studied and parameters that govern the generation of unsteady thrust were explored: namely chord-to-diameter and blade aspect ratios. Further simulation showed that the Darrieus rotor is prone to be locked in a deadband where the thrust is not continuous around a blade rotation. This discrete thrust is caused by the large variation of incidence angle during start-up making the Darrieus blade ineffective during part of the rotation.

The results show that unsteady thrust can be promoted through an appropriate selection of blade aspect and chord-to-diameter ratios, therefore self-starting rotors may be designed. A new definition of self-starting is also proposed.

List of Symbols

AR	Aspect ratio
B	Number of blades
c	Aerofoil chord
C_d	Drag coefficient
C_l	Lift coefficient
C_q	Torque coefficient
C_t	Tangential (or thrust) coefficient
D	Rotor diameter
D_f	Distance between blades

---

*Address all correspondence to this author.

k	Reduced frequency
R	Radius
S	Blade span
T_i	Torque
U	Headwind velocity
V	Free-stream velocity
W	Resultant velocity
α_D	Darrieus incidence angle
α_{pitch}	Pitch component of Darrieus incidence angle
α_{plunge}	Plunge component of Darrieus incidence angle
λ	Tip speed ratio
θ	Azimuth angle
ρ	Air density
ρ_m	Blade density
μ	Air viscosity
σ	Solidity
$I - IV$	Geometric quandrants
$1 - 4$	Aerofoil operating modes

INTRODUCTION

As energy demand grows, the use of small wind turbines has become increasingly attractive. Small wind turbines can be broadly categorised as horizontal-axis and vertical-axis, each having its own niche applications. In general, the latter is better suited to the urban environment where wind direction rapidly changes as it is insensitive to wind direction. However, Darrieus (vertical-axis) turbines are commonly believed to be non self-starting [1, 2].

Despite this perception, it has been increasingly reported that the turbine can self-start in even its simplest configuration of fixed-pitch, straight blades with a symmetrical aerofoil section [3–7]. These conflicting perceptions and observations indicates that there may be a physical aerodynamic mechanism which is not well understood.

Advances continue to be made in understanding of the physics of torque generation and starting behaviour. Hill et al [6] investigated the starting performance of a three-bladed H-rotor with NACA0018 blades, experimentally and numerically. Experimental wind-tunnel testing had demonstrated unaided startup in steady wind conditions. According to Hill et al, there are four main processes taking place during startup (Fig. 1b). The first process is an acceleration in which the turbine rotational speed linearly increases with time (1st acceleration). The turbine then enters its idling period when the rotor speed remains almost constant (plateau or deadband). In this process, turbine rotational speed increases but only very slowly. After a long period of idling, the rotor then accelerates rapidly (2nd acceleration) to a tip speed ratio of three or more and enters its steady operating state.

However the numerical modelling carried out by Hill [6] was based on steady aerofoil characteristics and could not predict the escape of the rotor from the plateau into the second acceleration zone. This discrepancy suggested that the modelling assumptions oversimplified the physical mechanisms inherent in the machine. The fundamental physics of starting must be explored in order that proper modelling assumptions can be made.

To address this issue, a physical explanation of starting behaviour based on an analogy between the aerofoil in Darrieus motion and flapping-wing mechanisms was proposed by Worasinchai et al [8]. The investigation involved a decomposition of the Darrieus incidence angle into two separate angles; a pitch angle variation and a plunge angle variation. The motion of blade rotation at low speeds could then be represented by flapping motion and this introduced an analogy to be made with bird flight. This analogy stresses the importance of unsteady effects which had been revealed by previous work on flapping wings [9].

With this analogy, knowledge of flapping-wing flow mechanisms was applied to understand thrust generation over the Darrieus flight path and the physics of self-starting. Worasinchai's analysis had shown that torque generation of the Darrieus rotor can be divided into two states: combined lift- and drag-driven and fully lift-driven states. The latter which is also called the flapping-wing analogy can be further divided into discrete and continuous thrust producing modes. This mode change (shown in Fig. 8) is closely related to a bird gait change from low to high flying speeds (take-off capability) (Fig. 2).

During take-off, birds typically perform specific techniques to generate lift and thrust. This includes changing wing shape, spreading the wing, reducing stroke amplitude, and increasing wing beat frequency. In the Darrieus context, this implies an optimisation of aerofoil section, an increase of aerofoil chord, a decrease of rotor diameter, and an increase of number of blades would produce a rotor design that would be more likely to self-start.

The present work presents the following novel elements:

1. Since no suitable data set existed: unsteady data on three aerofoils at the correct Reynolds numbers for wind turbine startup was collected and is presented in this paper.
2. Unsteady effects are incorporated into a Darrieus rotor start-up analysis.
3. The fundamental physics of starting are examined.
4. The impact of rotor configuration on starting capability is determined.

THEORY

The sign convention used in this paper is shown in Fig. 3, azimuth angle (θ) is divided into four segments: $I - IV$. The Darrieus incidence angle can be obtained as follows,

$$\alpha_D = \arctan\left[\frac{\sin\theta}{\lambda - \cos\theta}\right] \tag{1}$$

where λ is the tip speed ratio and θ is the azimuth angle. At high tip speed ratios this angle remains small but during startup this angle will take values from $-180°$ to $+180°$. The Reynolds number for the blade is obtained from:

$$Re = \left[\frac{\rho V c}{\mu}\right] \times \sqrt{\lambda^2 - 2\lambda\cos\theta + 1} \tag{2}$$

where the relative velocity experienced by the blade, W is given by $V \times \sqrt{\lambda^2 - 2\lambda\cos\theta + 1}$. The reduced frequency (effectively a ratio of how long the unsteadiness lasts for the time taken for this unsteadiness to convect over the object under consideration) is given by:

$$k = \frac{\omega c}{2W} \tag{3}$$

which can be expressed in terms of tip speed ratio to give:

$$k = \left[\frac{c}{D}\right] \times \left[\frac{\lambda}{\sqrt{\lambda^2 - 2\lambda\cos\theta + 1}}\right] \tag{4}$$

If a suitable data set of lift and drag coefficients at different incidence angles, Reynolds numbers and reduced frequency is available the thrust coefficient is found by resolving the forces into the circumferential direction:

$$C_t = C_l(\alpha_D, Re, k)\sin\alpha_D - C_d(\alpha_D, Re, k)\cos\alpha_D \tag{5}$$

The driving torque generated by each blade is then

$$T_i = \left(\frac{1}{2}\rho c S W^2\right) \times C_t \times R \tag{6}$$

The net driving torque produced by the rotor is a summation of the torques from all the blades attached to the rotor.

The incidence angle (α_D) can be shown to follow a sine-like curve above a unity tip-speed ratio as seen in Fig. 4. However the curve is not perfectly sinusoidal suggesting that the motion can be decomposed into further components and not only pitch. The decomposition into pitch and plunge angles was described in detail by [8] and is shown in Fig. 5.

Further analysis shows that the deviation is due to the change of translational speed that the aerofoil experiences when moving along its rotational path ($U - V\cos\theta$) (Fig 5). This change in translational speed effectively induces an additional velocity normal to the aerofoil and the aerofoil experiences heave (or plunge) movement, effectively making the Darrieus blades operate with a "combined" pitch and plunge motion. This kind of motion is typically referred as "flapping foil" which is analogous to the mechanism that birds employ to generate propulsion.

The following equations are applied to calculate pitch and plunge components.

$$\alpha_{pitch} = \arctan\left(\frac{\sin\theta}{\lambda}\right) \tag{7}$$

$$\alpha_{plunge} = \arctan\left(\frac{\sin\theta\cos\theta}{\lambda^2 - \lambda\cos\theta + \sin^2\theta}\right) \tag{8}$$

where α_D is incidence angle of the Darrieus motion, α_{pitch} is the pitch component, and α_{plunge} is the plunge component. An example of the decomposition is shown in Fig. 4 for $\lambda = 1.2$.

FLAPPING MOTION AND BIRD FLIGHT

Based upon the analogy and the decomposition of Darrieus incidence angle [8], the Darrieus flight path can be divided into an effective upstroke and downstroke which is shown in Fig. 6 and a flapping motion can be plotted.

Figure 7 shows an example of the flapping motion during the first quadrant (the azimuth angle (θ) from $0°$ to $90°$) together with a summary of flow physics involved.

It can be seen from Fig. 7 that the aerofoil is flapping up and the incidence increases. Although the flow is attached in the first region of the upstroke, the thrust force is small. This small force is due to the fact that the incidence angle is low and the lift force generated is nearly perpendicular to the aerofoil. The aerofoil continues to move and the incidence angle increases and finally exceeds the stall angle. However, the formation of a leading edge vortex delays the stall and promotes more negative pressure on the suction side and, hence, more lift and thrust. This process continues until the aerofoil reaches the end of upstroke. A detailed discussion of the motion over all the quadrants can be found in [10].

The analogy of flapping motion and Darrieus turbine operation can be used in the deadband and the second acceleration zone. In flapping flight, birds perform specific techniques to generate lift and thrust. Studies on bird locomotion have shown that birds generate different wake structures when flying at low and high speeds [11]. The wakes are caused by different wingbeat patterns: figure-of-eight and elliptical respectively (Fig. 8).

One of the main differences between these two patterns is the driving force generated throughout the stroke. While lift and thrust are continuously generated in the elliptical pattern, the forces are "discrete" in the figure-of-eight pattern and only produced during downstroke. In general, the figure-of-eight pattern has a longer downstroke (about two thirds of the total cycle [13, 14]). The relative timing and the pattern changes with increasing flying speed. If the speed is sufficiently high, wings during their upstroke will become effective in producing lift and thrust. The wingbeat then becomes an elliptical pattern in which each stroke lasts approximately the same time (Fig. 8).

The figure-of-eight pattern is used at low flying speeds, in particular during take-off. In order to maximise the driving force during the downstroke, birds typically flap their wings very fast (increasing reduced frequency), spread their wings as much as possible (increasing effective chord length), and sweep their wings forward (increasing the duration of force production). They also fold and retract their wings during the upstroke to reduce air resistance.

This flapping technique suggests that, in order to improve the turbine's ability to self-start, a Darrieus blade should:-

1. be effective in generating thrust during the downstroke
2. produce less drag (or less negative thrust) during the upstroke
3. have a short recovery period in order to promote more continuous thrust generation
4. exhibit a long downstroke phase at low tip speed ratios in order that a significant amount of thrust can be generated

The aerofoil in Darrieus motion exhibits an asymmetry of the relative timing of the upstroke and the downstroke and inherently provides a longer downstroke phase at low tip speed ratios (the peak of Darrieus incidence angle occurs before the azimuth angle of $90°$ and the negative peak occurs after the azimuth angle of $270°$ (Fig. 4)). The fourth requirement is then automatically satisfied.

For the simplest blade configuration where the blade is fixed, the first three requirements can be satisfied by selecting a suitable aerofoil profile and by properly sizing the rotor geometry. The effect of aerofoil choice is discussed in the next section.

EXPERIMENTAL SETUP

Unsteady data at the correct Reynolds number was required, since there was no suitable data set available in the open literature an experimental campaign was conducted to obtain the information.

Although the unsteady data required for Darrieus start-up analysis is a combined pitch and plunge motion, the motion considered in this investigation was a harmonically sinusoidal motion. The rationale for this is that the pitch motion is the dominant component and is relatively easy to generate in a wind tunnel environment. Pure pitch motion is less effective in generating vortex formation than the combined motion and it generally requires a higher reduced frequency to produce a vortex of comparable size. Based on the results in this paper the data obtained appears to have captured enough of the unsteady effects to allow an investigation into thrust generation during the start-up process.

Although a wider range of aerofoils were tested results from only three are shown in this paper, those being symmetrical (NACA0012), moderately cambered (SD7062), and highly cambered (S1223B) with the blunt trailing-edge modification, proposed by Standish and Van Dam [15]. The profile of each aerofoil is shown in Fig. 9, experiments were conducted from Reynolds numbers of 65,000 to 150,000 for four different cases: $1 - 4$ (Fig. 10) which were:-

1. normal mode (positive incidence range) with increasing incidence
2. normal mode (positive incidence range) with decreasing incidence
3. reversed camber mode (negative incidence range) with decreasing incidence
4. reversed camber mode (negative incidence range) with increasing incidence

The testing was conducted in the 0.5 m Plint wind tunnel at Durham University. The wind tunnel working section was configured to have a square cross-section (457 mm x 457 mm) with solid sides but open top and bottom (half-open) to minimise wall proximity effects. The motion was a sinusoidal pitching. It was generated by the use of crank mechanism which was powered by a 250 W D.C. motor.

All aerofoils had a span of 450 mm and a chord of 110 mm and were produced by rapid prototyping from Fullcure 720 material giving a high surface precision ($\pm$ 0.1 mm). Pressure measurements were taken using between 24 and 32 surface tappings with external pressure transducers connected via flexible tubing. A transfer function correction was applied to correct the transducer frequency response and attenuation. Unsteady pressure measurements were conducted for 2048 data points at 800 Hz which led to a certain number of cycles, depending on the aerofoil oscillation frequency (6 to 16 cycles for the lowest and highest oscillation frequencies, respectively). Lift and drag coefficients were then derived from the pressure data, the accuracy of the unsteady pressure coefficient (C_P) measurement was assessed as ± 0.16, for a typical aerofoil the C_P would vary between 1 and -6. More details on the experiments can be found in [10] including data from additional aerofoil geometries.

AEROFOIL PERFORMANCE CHARACTERISTICS

Figure 11 presents the time varying thrust (C_t) of the three aerofoils at a reduced frequency of 0.2. The C_t behaviour is also marked as state 1 to 4 to represent different motions during the wing-beat cycle (Fig. 11 and 12).

The motions in the Darrieus flight path are:-

1. The second half of the up-stroke (from 1 to 2), represented by a solid line with a triangle marking.
2. The first half of the down-stroke (from 2 to 3), represented by a solid line.
3. The second half of the down-stroke (from 3 to 4), represented by a solid line with upside down triangles.
4. The first half of the up-stroke or recovery region (from 4 to 1), represented by a solid line with open circles.

In terms of unsteady thrust, it is observed that the three aerofoils generate very different C_t characteristics. The symmetrical section can generate a positive thrust coefficient of around 0.15 in both modes of operation. Dynamic-stall angles of attack were about $20°$ and $-30°$ for normal and reversed mode, respectively.

Despite the fact that the NACA0012 aerofoil is symmetrical the unsteady data is asymmetrical especially in the normal-up and reversed-down mode. The difference between these two modes is attributed to interaction of the pitching motion and the incoming flow. In the normal mode, the vortex can be swept away by the incoming flow. In the reversed cambered mode the vortex is not significantly affected by the incoming flow and the vortex strength is nearly constant when travelling along the aerofoil chord. This results in a distinctly asymmetrical set of data for the NACA0012 despite the symmetrical geometry.

It can be seen that the use of cambered sections will shift the zero-lift angle of attack to the negative range, leading to a shift of the neutral point (or midstroke (states 1 and 3)) to the lower half of the circle. This effectively shortens the recovery region (the third requirement to promote self-starting).

Superior performance of the cambered sections is observed during stage 1 to 2 (Fig. 11). The positive thrust coefficient is significantly higher (about 0.3 and 0.45 for the SD7062 and the S1223B, respectively) and the stall angles are postponed to approximately 30° for both sections. In addition, the use of these cambered sections, which exhibit higher post-stall lift, also leads to less negative thrust during state 2 to 3 (the second requirement to promote self starting). This, together with the shortened recovery period (Fig. 12), makes the use of cambered aerofoils beneficial during the upstroke. A similar effect might be achieved by introducing a small pitch offset on a symmetrical section.

However, the cambered sections do not exhibit a clear positive thrust during state 3 to 4 (downstroke) which is the main thrust contributor at low tip speed ratios. A close examination of the pressure distribution has revealed that its leading edge shape has lost its "propulsive effect" during this mode of operation.

The measured pressure distribution in normal and reversed mode is shown in Fig. 13 and it can be seen that the propulsive effect is greatly influenced by the leading edge shape of the aerofoil. A propulsive effect (force from right to left in Fig. 13) can be easily generated in normal operation as the suction peak has a forward thrust component. This forward component is lost when operating with reversed camber mode since the leading edge shape is comparatively flat. This can be worse on the highly cambered sections as the pressure surface is "concave" and any pressure difference caused by vortex formation will not promote propulsion.

It is worth noting that this effect is further amplified by vortex formation under dynamic conditions [10]. The presence of the dynamic-stall vortex induces a higher suction peak which results in an additional forward thrust component. Additionally, its presence also delays stall up to a higher incidence angle, effectively increasing the range that the propulsive effect is present. This characteristic is one of the reasons why an additional propulsive force is created when operating under dynamic conditions. This unsteady propulsive force will be continuously generated if the aerofoil oscillates within the dynamic-stall angle range.

It is apparent from this performance comparison that the leading edge shape of the aerofoil is critical. In order to promote unsteady thrust in both modes of operation, the aerofoil must be able to generate suction peaks in both modes of operation. The addition of camber only increases the forward thrust component in the normal mode but decreases the thrust in the reversed camber mode.

The requirement of being able to generate a forward thrust component during both modes of operation makes the symmetrical aerofoil sections (i.e. the NACA0015 and NACA0018) a simple and attractive choice for Darrieus rotors. However, there is still room for improvement. It is likely that a small camber increase could be added to improve the aerofoil performance during upstroke but the maximum camber should be located closer to the trailing edge in order that the leading edge shape is still active in generating the forward thrust component when operating with reversed cambered operation.

THE INCLUSION OF UNSTEADY EFFECTS IN ROTOR ANALYSIS

For the reasons outlined above, performance modelling was restricted to the conventional NACA section. A numerical model was developed under the assumptions that:-

1. Wind speed is *steady* and *uniform* across the rotor swept area.
2. The turbine spins slowly during start-up and the effect of induced velocity is *negligible*.
3. There is *no* blade/wake interaction within the turbine and each blade is aerodynamically *independent*.
4. Effects of unsteadiness caused by a combined pitch and plunge motion can be represented by those caused by pure pitch motion.

Based upon these assumptions, the calculation of flow conditions that the blade experiences can be obtained through velocity triangle analysis. The consideration presented herein is based upon the sign convention defined in Figure 3.

Flow conditions (resultant wind speed, incidence angle, and reduced frequency) that the blade experiences depend upon the blade azimuth angle and its speed relative to the wind.

Modelling of the starting behaviour is based upon the approach of Dominy et al [4] which is carried out by stepping the time and tracking the blades over the flight path.

The calculation of torque at each time step depends on the reduced frequency that the blade experiences. As long as the reduced frequency is lower than 0.02, C_l and C_d are interpolated from look-up tables over a range of Reynolds numbers. If the reduced frequency is higher than 0.02 and the magnitude of the incidence angle is lower than 60°, unsteady effects are incorporated into the model by the use of the Leishman-Beddoes dynamic-stall model [16].

The experimental stall angles (which are a function of *Re* and *k*) were directly given to the Leishman-Beddoes model. This had the result of informing the model how long the unsteady effects prolong at a particular reduced frequency and Reynolds number. The circulation loss near the tip was taken into consideration by applying Prandtl's tip loss function to both ends of the blades. More detail of modelling can be found in [10] and a block diagram is provided in Fig. 18 in the Appendix of this paper.

Simulations were performed on the turbines tested by Hill et al [6], Rainbird [5], and Chua [3]. Table 1 summarises turbine geometric parameters. Figure 14 shows a comparison between the experimental data and the numerical simulations

based on the method presented here (labelled SIM in the figures). It is noted that the prediction of Chua's result was made using static lift and drag coefficients of a NACA0015 (the model needs both static and dynamic information), provided by Rainbird [5]. Dynamic parameters such as dynamic-stall angle were kept unchanged in all predictions.

Overall, the experimental and predicted results are in qualitative agreement and the overall behaviour of the starting is well-captured. In the first validation (Hill et al), discrepancies are observed in two areas: the plateau (between 60s to 140s) and the final, operating tip speed ratio that the rotor reaches (between 160s to 200s). The discrepancy in the plateau area is comparatively large and the model predicts that the rotor accelerates to a tip speed ratio of around 0.7 before decelerating, causing a λ plateau. The plateau is less evident in the Rainbird test and the rotor seems to accelerate continuously, though with a decreasing acceleration rate between 50s and 100s before reaching the second acceleration zone.

Over-prediction of the final, operating tip speed ratio is seen in both the Hill and Rainbird validation cases. The over-prediction is anticipated to be a result of bearing friction and windage of the blade support arm of the real machine which is assumed to be zero in the modelling. Another cause might be the effect of blade/wake interaction which is ignored in the model. The wake generated by the upstream blade might be expected to alter the flow that the downstream blade experiences and the assumption that each blade is aerodynamically independent might be invalid under this condition.

In Chua's case, it can be seen that the result is in good agreement for the entire starting process, particularly in the second zone; a region where the tip speed ratio increases with a decreasing acceleration rate (referred to as a plateau in Hill [6]). It is noted that over-prediction of the steady, operating region is small for this case. This was attributed to the the high drag in the wind-tunnel data provided by Rainbird as a result of a relatively poor manufacturing process [5]. An over-prediction would be present if other wind tunnel data is used.

All in all, the model with blade dynamic performance can predict the Darrieus rotor starting behaviour reasonably well and demonstrates a dramatic improvement over previous models. However, discrepancies between the experiments and the model prediction also suggests that there is still room for some improvement.

An obvious avenue for improvement would be to include the plunge component into the analysis which is currently neglected as collecting data from a combined pitch and plunge motion is challenging. The current analysis also does not examine how a turbulent inflow influences Starting performance. Although the authors have no data on this scenario it is plausible to expect that with both an earlier laminar-turbulent transition and an increase in the level of unsteadiness the ability of the rotor to self start would be enhanced.

FUNDAMENTAL PHYSICS OF STARTING

Figure 15 presents Darrieus turbine starting behaviour together with variations of flow conditions that the blade experiences during the starting process.

During the first acceleration, the Reynolds number that the blade experiences is around 33,000 when stationary, varying over the flight path when the rotor rotates. Minimum and maximum values occur at azimuth angles of 0° and 180°, respectively. Since the tip speed ratio is lower than one, incidence angle variation in this region is still large and the blade experiences all possible angles of attack ($\pm 180°$) (Fig. 15b). The rate of incidence change gradually increases with increasing tip speed ratio. It is worth noting that the driving thrust generated by the blade is alternately driven by drag and lift (drag-driven state occurs in quadrant IV and I due to an extremely large incidence angle. The lift-driven state occurs in quadrant II and III). Quasi-steady and transient predictions are in good agreement up to a tip speed ratio of around 0.3.

Above the tip speed ratio of 0.3, the transient effect is present and plays a role in driving the rotor. This transient effect is significant when the aerofoil is not fully stalled (normally in the incidence range of $\pm 45°$) [10]. Consideration of incidence variation indicates that this occurs in quadrant III and it is, therefore, the blade in quadrant III that provides an additional thrust to drive the rotor in this region. It is also observed that the Reynolds number variation increases with increasing tip speed ratio and periodically approaches zero at the unity tip speed ratio. The blade in these two quadrants is therefore less effective in producing thrust, causing the rotor acceleration to fall (Fig. 15a).

The rotor will enter a fully lift-driven state (flapping-wing analogy) at the unity tip speed ratio. The driving force in quadrants I and IV which was previously generated by drag has now changed to be generated by lift. With an incidence range that is still large (for example, $\pm 64°$ at λ = 1.1) and with low Reynolds number in quadrant IV and I, the blade in these quadrants is still not effective in driving the rotor and it is operation in quadrant III that provides most of the drive, leading to a "discrete" thrust generation and a comparatively low driving force. With the slowly increasing tip speed ratio, the incidence range slowly reduces and the Reynolds number range slowly increases (Fig. 15b and c).

The discrete thrust-producing state continues until the rotor reaches a significantly higher tip speed ratio (around 1.5 to 2). At this tip speed ratio, the lowest Reynolds number at the azimuth angle of 0° is increased to around 33,000 and the incidence range becomes small ($\pm 30°$). The blade in quadrant I becomes active again in generating thrust. The rotor then takes off to a steady, operating tip speed ratio of around 3.4 where Reynolds number variation has jumped to lie in the range from 66,000 to 131,000 and the incidence angle variation is between $\pm 20°$.

EFFECTS OF ROTOR GEOMETRY

As implied by the flapping wing analogy, the rotor geometry including chord-to-diameter ratio (c/D) and blade aspect ratio (AR) will influence on the turbine's ability to start. A parametric study was conducted to explore this in detail.

The investigation was made by defining rotors to have different diameters and spans. The blade chord length (c) was changed to obtain c/D ratios between 0.03 and 0.14. For a specific diameter and span, c/D and AR are connected and a modification of one parameter will affect the value of another. Different span lengths were simulated to cover blade aspect ratios between 4.29 and 40. All simulations were performed at a wind speed of $6\,\mathrm{ms}^{-1}$. The blade material (ρ_m) was assumed to be the same as Hill's rotor [6] and used to calculate rotor inertia. A total of fifty two different rotor geometries were simulated and the full set of results can be found in [10].

Figure 16 shows the results in the form of two 3D scatter plots with c/D and AR making up the x and y directions. The left hand figure has λ on the z axis and the right hand figure has T_s on the vertical scale. The maximum simulation time was 200 seconds and any rotor that could accelerate out of the plateau within this simulation time was marked as self-starting and is represented by the large red symbols in Fig. 16. Rotor geometries that do not self start have a T_s value of 200 s and are marked by the smaller blue symbols. A small cross symbol indicates the projection of the rotor geometry onto the walls of the 3D box to aid interpretation of the figure.

Figure 16 shows clearly that the rotor geometry is a key factor in starting performance. In general, any rotor that has a c/D ratio of 0.05 or less will not start whatever the value of blade aspect ratio; a direct result of the small chord length that leads to a small Reynolds number when stationary. With an increment of the c/D ratio to around 0.10, the Reynolds number is sufficiently high for the rotor to be able to generate sufficient torque to start spinning. The Reynolds number is critical since if it is too low, the aerofoil will suffer performance degradation (for example, its lift curve slope will be significantly reduced in comparison to a high Reynolds number [17], leading to a very small torque). The rotor, however, cannot take off to a high tip speed ratio as the level of unsteadiness created by this c/D ratio is still low and the additional, unsteady thrust is not effectively generated.

With a c/D ratio above 0.12, the reduced frequency increases sufficiently for unsteady thrust to be generated. This unsteady thrust drives the rotor through the startup period and the rotor manages to take off to its steady operating tip speed ratio of around 3. A further increase of c/D ratios to 0.14 shortens the blade aspect ratio and the time that the rotor takes to take off is decreased. It is also observed that rotors that have too small a span length will not start although the c/D ratio is high.

With increasing diameter, the rotor tends to have a difficulty starting. This increase imposes two effects on the rotor. Firstly, it increases the rotor inertia and, at a certain value of diameter, rotors will fail to start. Secondly, with regard to our flapping analogy, the large diameter causes a large stroke amplitude which leads to a slow rate of flapping. The distance that the blade has to travel to begin a new stroke can be calculated from

$$D_f = \frac{\pi D}{B} - c \tag{9}$$

So for example rotors which have the same c/D ratio of 0.12, end up with a D_f between 0.473 m and 0.927 m. This indicates that the blade in the latter case has to travel twice as far to enter the area where thrust is generated.

Based upon the simulation results it is possible to design rotors that self-start. Rotors self-start in the following ranges: $0.5\,\mathrm{m} \leq D \leq 0.75\,\mathrm{m}$, $0.12 \leq c/D \leq 0.14$ and $5.71 \leq AR \leq 16.7$. Though clearly these results depend on the choice of aerofoil for the turbine. Woransinchai [8] observed that many of the early Darrieus turbines were constructed with low c/D ratios and the lack of unsteady thrust explains their inability to self-start.

All of the simulated rotors have a comparatively low inertia and this promotes the ability to start. Using lightweight materials may allow the range of self-starting rotor configurations to be significantly expanded.

SYSTEM PERFORMANCE

The torque characteristic of the Darrieus rotor is predicted and presented in Fig. 17. It can be seen that the torque generated (C_q) by the rotor is comparatively high when stationary before decreasing with increasing tip speed ratio reaching a minimum around $\lambda = 1$. Above $\lambda = 1$, C_q increases until it reaches its peak at a tip speed ratio of 2.5 before decreasing.

The effect of the generator and the load on the turbine starting capability can be easily observed by plotting the Darrieus torque characteristic together with resistive torque posed by the generator and the load. (Fig. 17). When the cogging torque is high, the net torque can be negative in the first two regions (first acceleration and deadband) and the turbine will not accelerate. Generators that have no cogging torque are available [18] and this generator type will aid self-starting.

In addition to the cogging torque, the resistive torque created by the load is also of importance. If the resistive torque is increased too quickly, the net torque could be negative and will trap the turbine in the plateau (Fig. 17). Careful matching

between the turbine and the load will also promote the turbine's ability to self-start.

SELF-STARTING DEFINITION

The investigations conducted so far also raises a question of how self-starting should be defined. Previous researchers had defined that the turbine is self-starting when it can accelerate from rest to the point that a significant power has been produced [19, 20]. This definition is load-dependent and the term "significant power" is imprecise.

There exist circumstances that power can be generated while the machine has not reached its final operating point. One of the clearest cases is with a resistive heating load in which heat will be generated as soon as the machine spins. With the resistive torque that increases continuously with increasing tip speed ratio, it is likely that the net torque will be small or even negative at the tip speed ratio of around 1 and the turbine will not further accelerate (Fig. 17). Under this condition, the turbine has not reached its ideal operating point but can produce some power. As a consequence, the self-starting should not be defined in terms of power.

Another specific definition had been proposed in terms of tip speed ratio. Lunt [21] defined that the machine is deemed to have started if it has accelerated from rest to a condition where the blade operates at a steady speed that exceeds the wind speed (tip speed ratio of 1) as he believed that the machine will further accelerate once the machine has been driven by lift. However, this present investigation has shown that, although the blade operation has shifted from the combined lift- and drag-driven to fully lift-driven at this tip speed ratio, the torque coefficient is at its minimum and the machine is prone to be locked in the deadband. The change from combined to full lift-driven state is therefore not a guarantee that the machine will continue to accelerate.

A possible definition that covers the whole process is one based on the concept of acceleration from rest to the final operating tip speed ratio. The final operating tip speed ratio, however, depends on a number of parameters such as free-stream wind speed, rotor configuration, aerofoil employed, and the load that the machine is connected to. Wind tunnel investigations by Reynolds [7] have shown that, for a specific rotor configuration (the rotor tested is the same as that tested by Hill et al [6]), the final tip speed ratio increases with increasing free-stream wind speed (increased aerodynamic torque). It also decreases with increasing resistive load. In essence, the resistive load will make the turbine reach a lower tip speed ratio where the incidence range is higher. With increasing resistive torque, the operating tip speed ratio decreases and, if the resistive torque is too high, the machine will fall into the deadband region.

In the light of this information, it is proposed that an H-Darrieus turbine is said be self-starting if:-

"The turbine can accelerate from rest to the tip speed ratio where thrust is continuously generated over the Darrieus flight path. Its final operating tip speed ratio will be an equilibrium point where aerodynamic and resistive torques match."

CONCLUSIONS

1. Unsteadiness is an inherent property of the Darrieus rotor start-up.
2. A series of experiments have been conducted to obtain unsteady data at the relevant Reynolds numbers and reduced frequency for Darrieus turbine start-up.
3. Incorporation of blade dynamic performance into the analysis has improved the prediction of Darrieus turbine starting behaviour. The prediction tool has been validated against available test cases and shows good agreement.
4. The additional unsteady thrust can be exploited to promote the turbine's ability to start.
5. The unsteady thrust generation is directly related to the rotor geometry, namely aerofoil section, diameter, chord-to-diameter ratio, and blade aspect ratio.
6. The aerofoil shape is vitally important, particularly the leading edge shape as it promotes propulsive effects. Aerofoils with a high percentage of camber will lose their effectiveness in producing forward thrust when operating in the reversed camber operation.
7. Symmetrical NACA sections remain a simple and attractive choice for Darrieus rotors.
8. To effectively promote the propulsive effects of the aerofoil, the blade chord should be sufficiently large in comparison to rotor diameter. Simulation results show that there exist a range of design parameters for which a rotor will have an ability to start.
9. Self-starting should be defined in terms of thrust generation. The turbine is said to be self-started when thrust is generated continuously over the Darrieus flight path.

The investigations presented here provide a resolution to the contradictory accounts of whether or not the H-Darrieus turbine has the potential to self-start. The H-Darrieus turbine *can* be made to self-start however whether a particular rotor self-starts or not depends upon a number of issues including the rotor aerodynamics, the choice of materials, the generator technology and the suitable matching between the rotor and the load. Key to this understanding is that the unsteady aerodynamics need to be considered before an accurate prediction of starting behaviour can be obtained.

References

[1] Kentfield, J. A., 1996. *The Fundamentals of Wind-driven Water Pumpers*. Taylor and Francis, London.

[2] Ackermann, T., and Soder, L., 2000. "Wind energy technology and current status: a review". *Renewable and Sustainable Energy Reviews,* **4**, pp. 315–374.

[3] Chua, K. L., 2002. Design and Testing of a Vertical Axis Wind Turbine Rotor. Bachelor project, Faculty of Mechanical Engineering, University of Technology, Malaysia.

[4] Dominy, R., Lunt, P., Bickerdyke, A., and Dominy, J., 2007. "The Self-starting Capability of a Darrieus Turbine". *Proc. IMechE., J. Power and Energy,* **221**, pp. 111–120.

[5] Rainbird, J., 2007. "The Aerodynamic Development of a Vertical Axis Wind Turbine". MEng thesis, School of Engineering, Durham University, England.

[6] Hill, N., Dominy, R., Ingram, G., and Dominy, J., 2008. "Darrieus Turbines: the Physics of Self-starting". *Proc. IMechE., J. Power and Energy,* **226**, pp. 21–29.

[7] Reynolds, K., 2010. "VAWT Start Up Characteristics". Technical report, School of Engineering, Durham University, England.

[8] Worasinchai, S., Ingram, G., and Dominy, R., 2012. "The Physics of H-Darrieus Turbine Self-starting Capability: Flapping-wing perspective". *ASME Turbo Expo 2012, June 11-15, Copenhagen, Denmark*(GT2012-69075).

[9] Dickinson, M., 1996. "Unsteady Mechanisms of Force Generation in Aquatic and Aerial Locomotion". *AMER. ZOOL,* **36**, pp. 537–554.

[10] Worasinchai, S., 2012. "Small Wind Turbine Starting Behaviour". PhD thesis, School of Engineering and Computing Sciences, Durham University, England. Online at: `http://etheses.dur.ac.uk/4436/`.

[11] Tobalske, B., 2000. "Biomechanics and Physiology of Gait Selection in Flying Birds". *Physiological and Biochemical Zoology,* **73(60)**, pp. 736–750.

[12] Tobalske, B., and Dial, K., 1996. "Flight Kinematics of Black-billed Magpies and Pigeons over a Wide Range of Speeds". *Journal of Experimental Biology,* **199**, pp. 263–280.

[13] Alexander, D., 2002. *Nature's Flyers: Birds, Insects, and the Biomechanics of Flight*. The Johns Hopkins University Press Series.

[14] Biewener, A., 2003. *Animal Locomotion*. Oxford Animal Biology Series, OUP Oxford.

[15] Standish, K., and Van Dam, C., 2003. "Aerodynamic analysis of blunt trailing edge airfoils". *ASME Journal of Solar Energy Engineering*.

[16] Leishman, J. G., 2006. *Principles of Helicopter Aerodynamics* . Cambridge University Press; 2 edition.

[17] Selig, M., Guglielmo, J., Broeren, A., and Giguere, P., 1996. "Experiments on Airfoils at Low Reynolds Numbers". *34th Aerospace Sciences Meeting & Exhibit, January 15-18, 1996, Reno, NV*.

[18] Bumby, J., Stannard, N., and Martin, R., 2006. "A Permanent Magnet Generator for Small Scale Wind Turbines". In Proceedings of the 17th International Conference on Electrical Machines, Chania, Crete, Greece.

[19] Ebert, P., and Wood, D., 1997. "Observations of the Starting Behaviour of a Small Horizontal-axis Wind Turbine". *Journal of Renewable Energy,* **12**, pp. 245–257.

[20] Kirke, B., 1998. "Evaluation of Self-starting Vertical Axis Wind Turbine for Stand-alone Applications". PhD thesis, School of Engineering, Griffith University, Australia.

[21] Lunt, P. A., 2005. "An Aerodynamic Model for a Vertical-axis Wind Turbine". MEng thesis, School of Engineering, University of Durham, England.

APPENDIX

A block diagram of the method used to calculate the starting behaviour is found in Fig. 18.

Table 1.   TURBINE CONFIGURATIONS

Configuration	Hill et al and Rainbird	Chua
Number of blades (B)	3	3
Aerofoil	NACA0018	NACA0015
Chord (m)	0.083	0.070
Span (m)	0.6	0.5
Radius (m)	0.375	0.25
Inertia ($kg - m^2$)	0.018	0.015
Solidity (σ) (-)	0.664	0.84
Chord-to-diameter ratio (-)	0.11	0.14
Blade aspect ratio (AR) (-)	7.229	7.143

List of Figures

Fig. 1. DARRIEUS TURBINE STARTING BEHAVIOUR (REPRODUCED FROM [3] AND [6]). GTP-15-1321
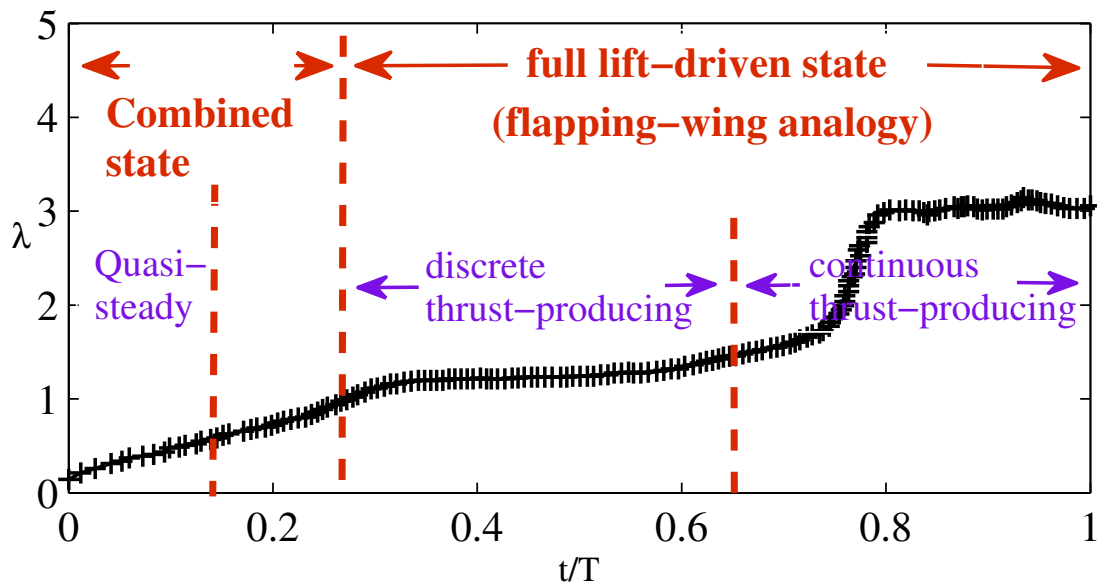
Fig. 2. THRUST-PRODUCING STATES AT STARTUP (REPRODUCED FROM [8]) GTP-15-1321
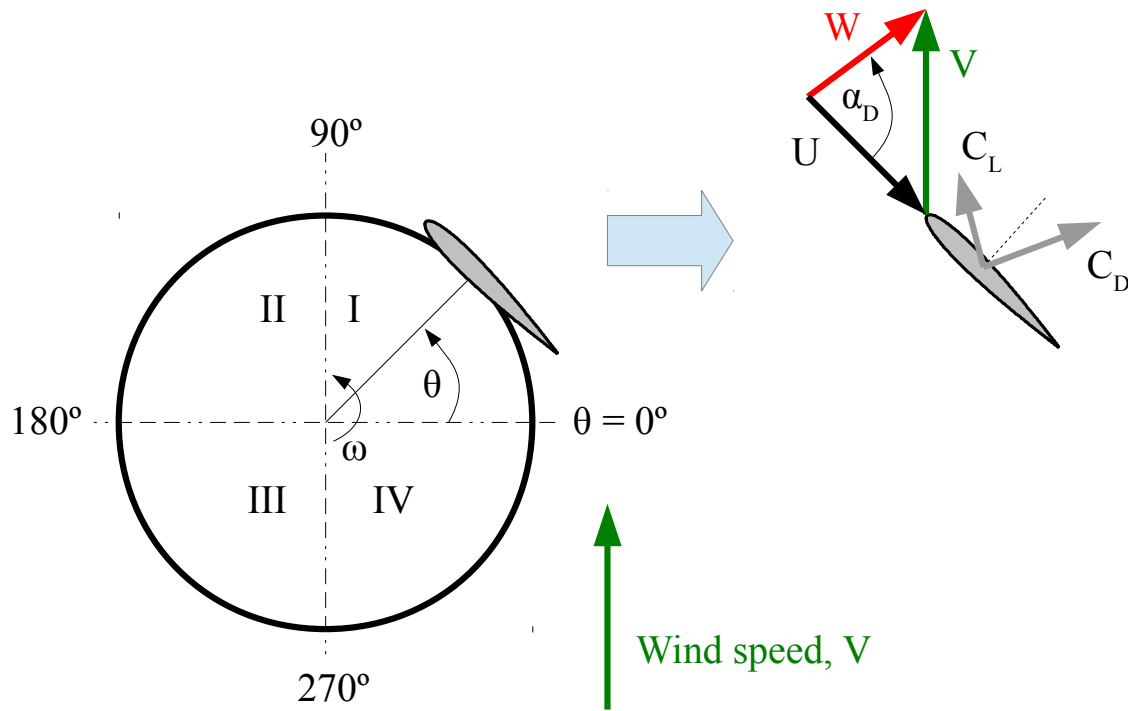
Fig. 3.   SIGN CONVENTION GTP-15-1321
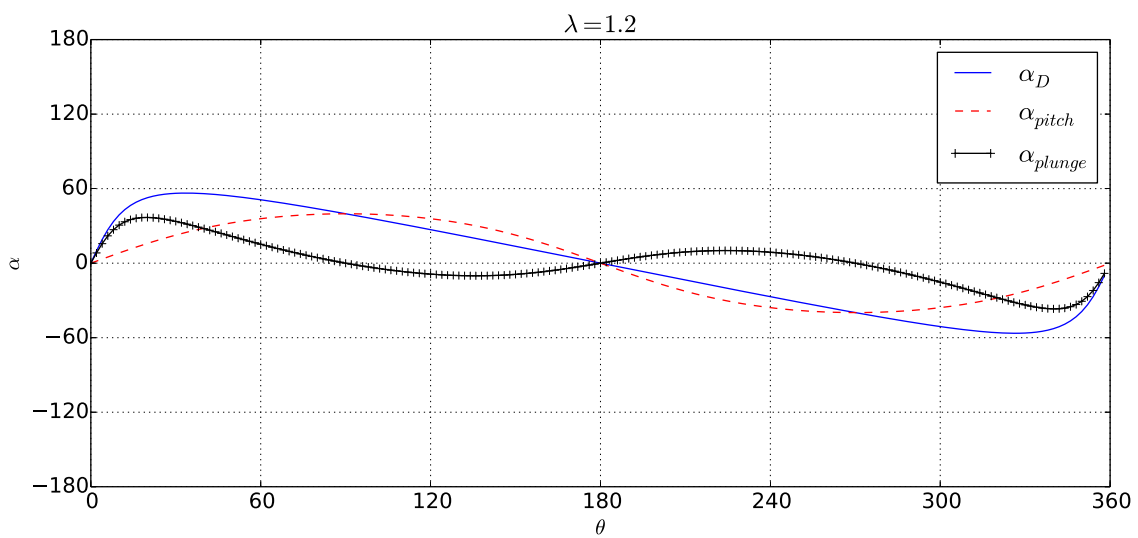
Fig. 4.   PITCH AND PLUNGE COMPONENTS GTP-15-1321
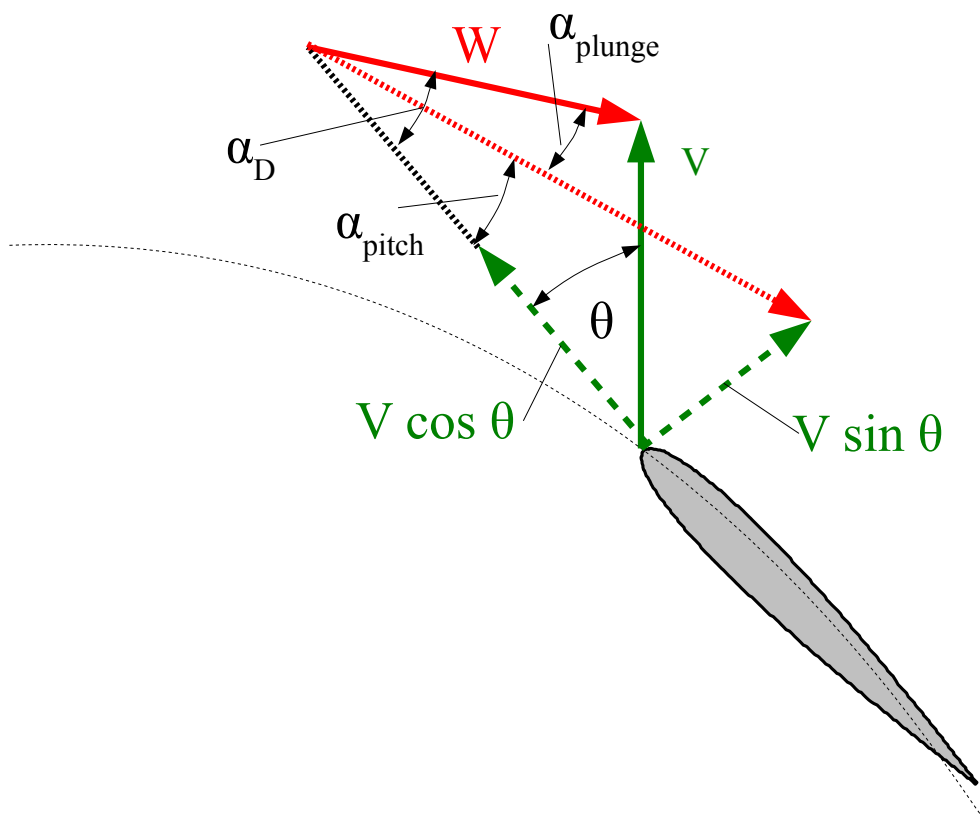
Fig. 5.   PITCH AND PLUNGE ANGLES GTP-15-1321
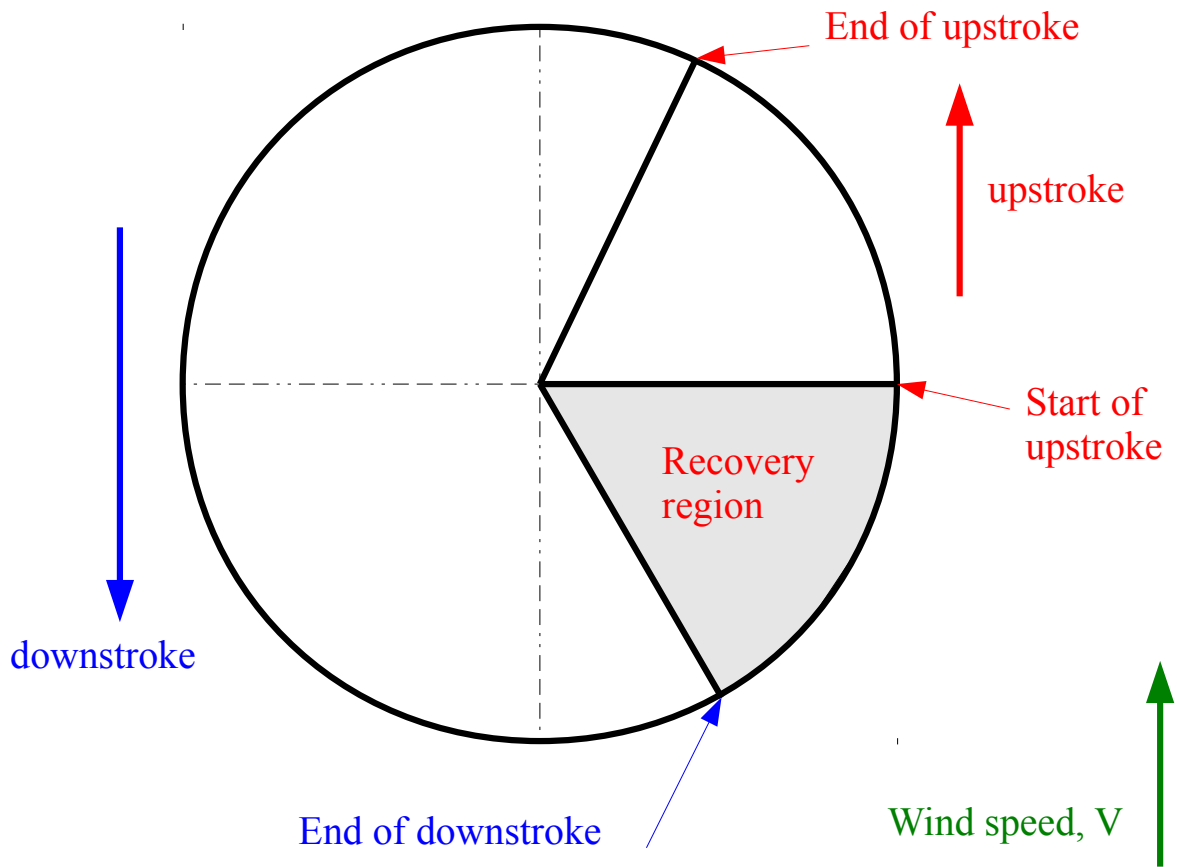
Fig. 6.   DARRIEUS FLIGHT PATH AND ITS ANALOGY TO FLAPPING WINGS GTP-15-1321
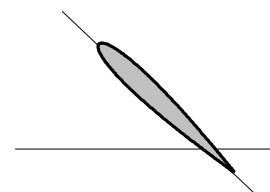
Vzimuth angle	Pitch	Plunge	Flow Features	Aerofoil Motion
$\theta = 0^\circ$	Neutral	Neutral	Unstalled flow $\alpha_D = 0^\circ$	
$0^\circ < \theta < 30^\circ$	Increasing	Increasing	Leading edge vortex formation Delayed stall $0^\circ < \alpha_D = 34^\circ$	
$\theta = 30^\circ$	Increasing	Maximum (positive)	Leading edge vortex formation Delayed stall $\alpha_D = 34^\circ$	
$30^\circ < \theta < 90^\circ$	Increasing	Decreasing	Vortex convection $\alpha_{D,max} = 38^\circ$	

Fig. 7.   AEROFOIL MOTION GTP-15-1321
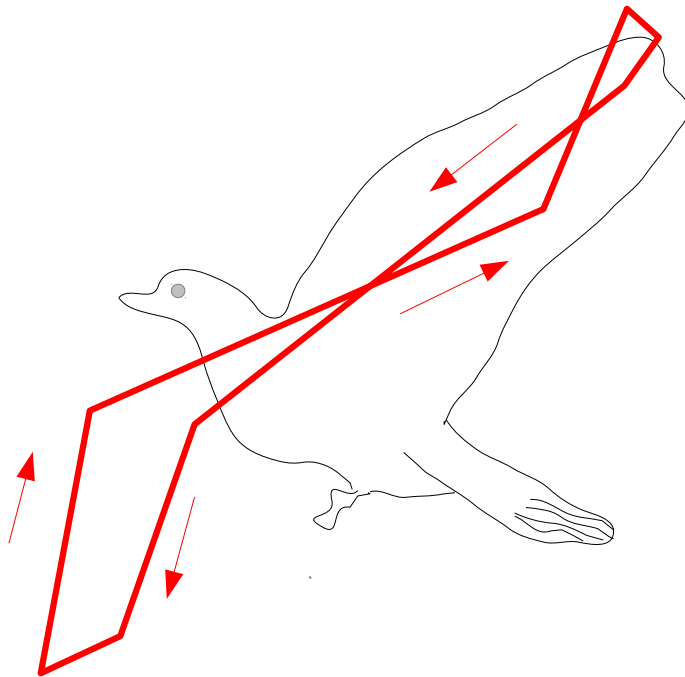
(a) Figure of eight pattern,
discrete thrust, low speed flight
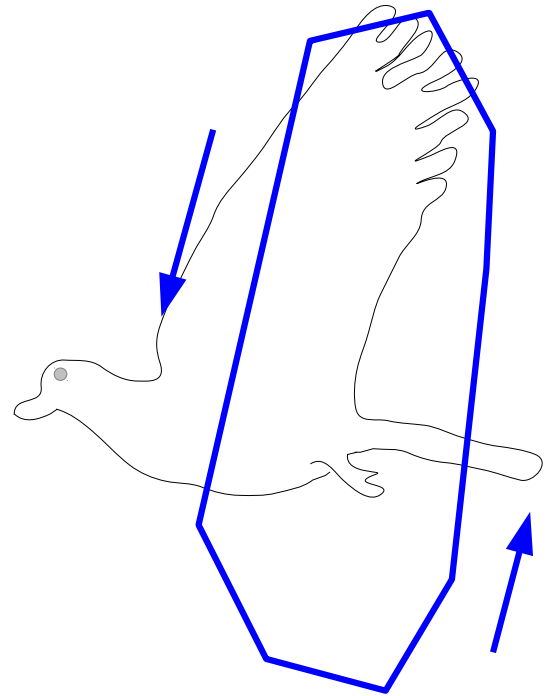
(b) Elliptical pattern,
continuous thrust, high speed flight

Fig. 8.   WINGBEAT PATTERNS (ADAPTED FROM [12]). GTP-15-1321

NACA0012

SD7062

S1223B

Fig. 9. AEROFOILS USED IN THIS PAPER GTP-15-1321
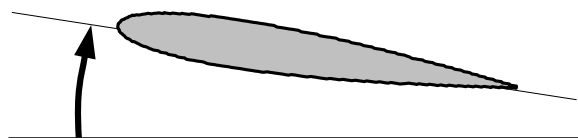
1. Normal mode with increasing incidence
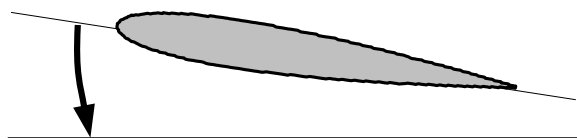
2. Normal mode with decreasing incidence
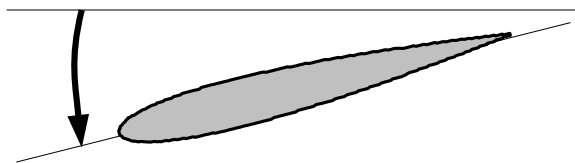
3. Reversed camber mode with decreasing incidence
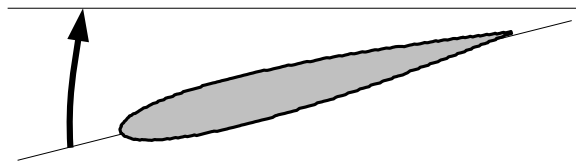
4. Reversed camber mode with increasing incidence

Fig. 10.   AEROFOIL MOTION TESTED GTP-15-1321
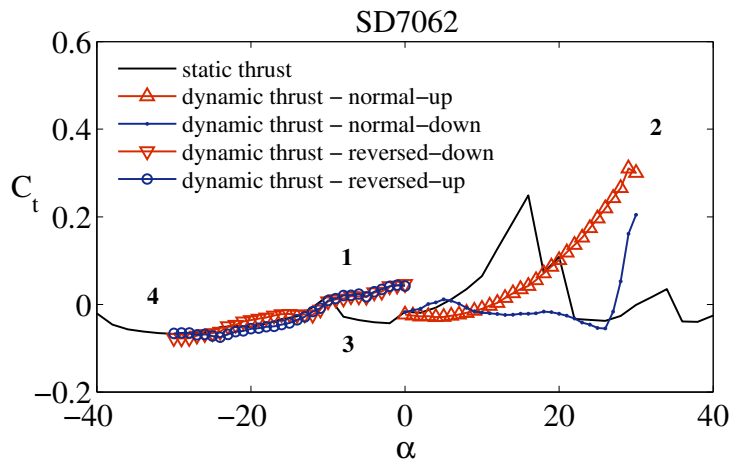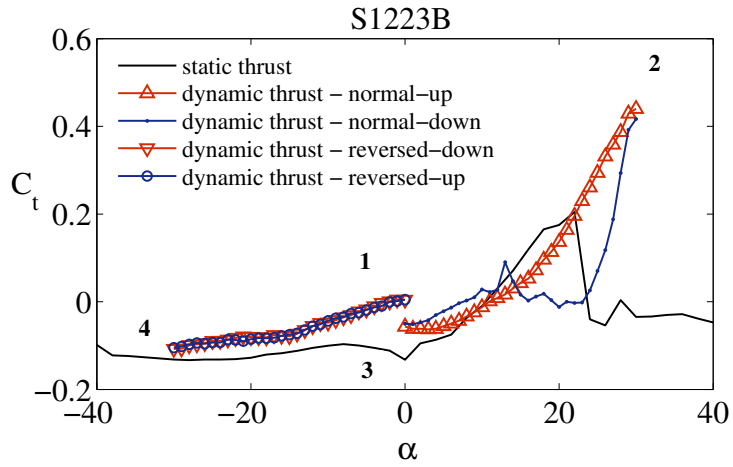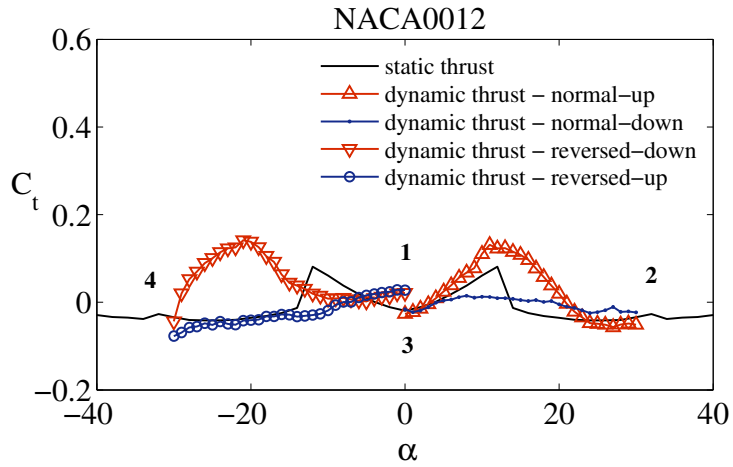
Fig. 11.　THRUST COEFFICIENTS GTP-15-1321
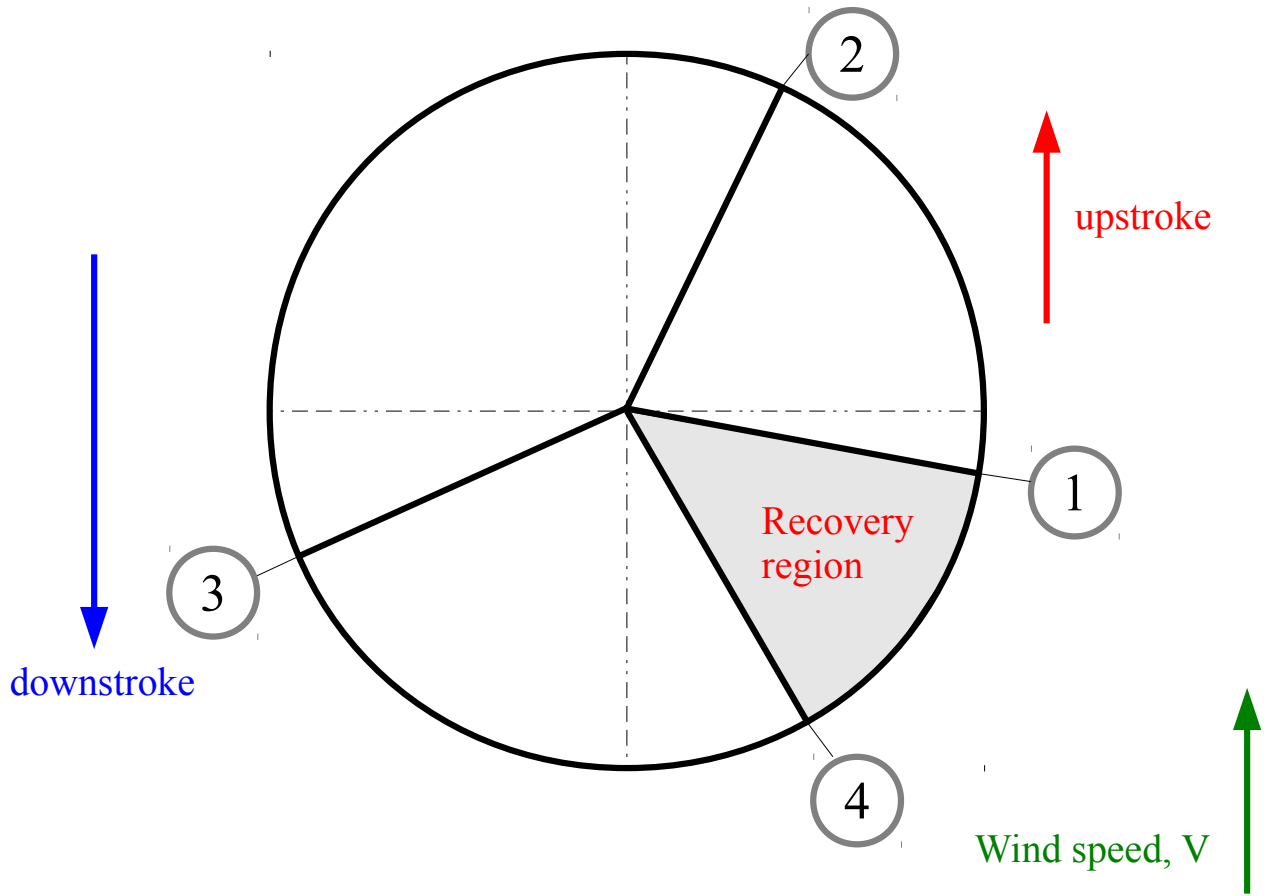
Fig. 12.   THE SHIFT OF MIDSTROKE DUE TO A CAMBERED AEROFOIL SECTION GTP-15-1321
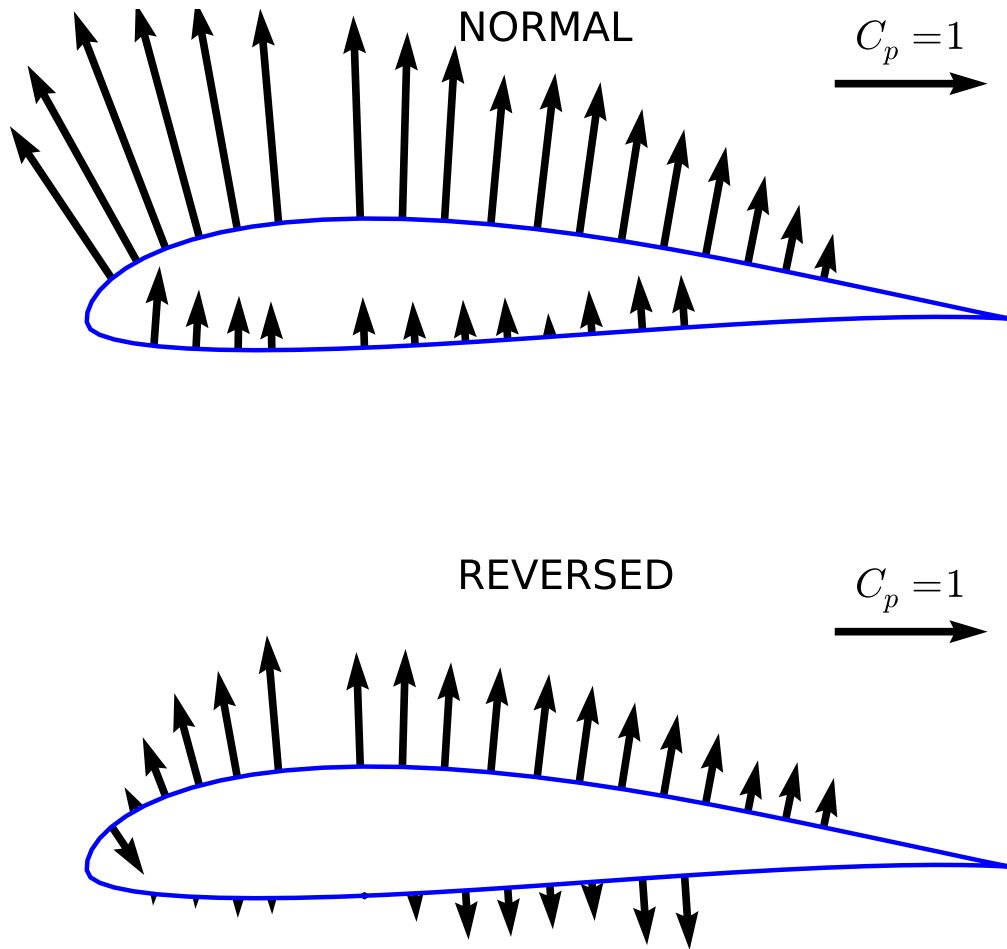
Fig. 13.   PRESSURE DISTRIBUTION OVER SD7062 IN NORMAL AND REVERSED MODE AT $15°$ INCIDENCE ($Re = 90,000, k = 0.2$)
GTP-15-1321
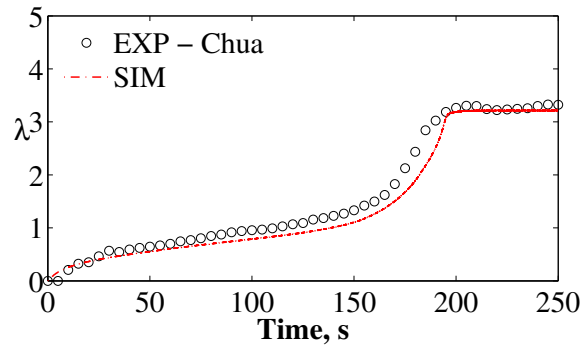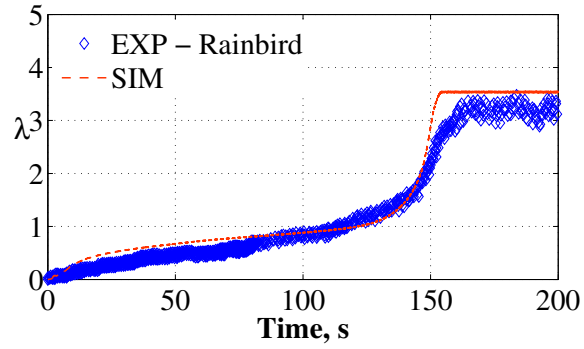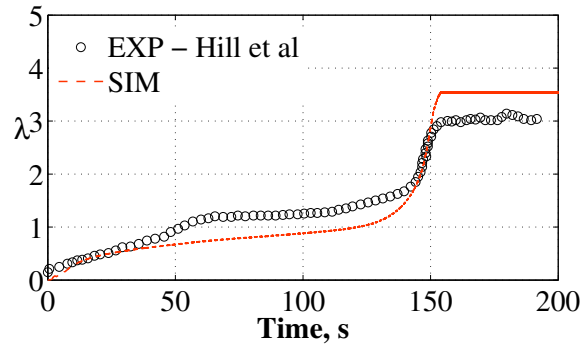
Fig. 14. STARTING BEHAVIOUR VALIDATION GTP-15-1321
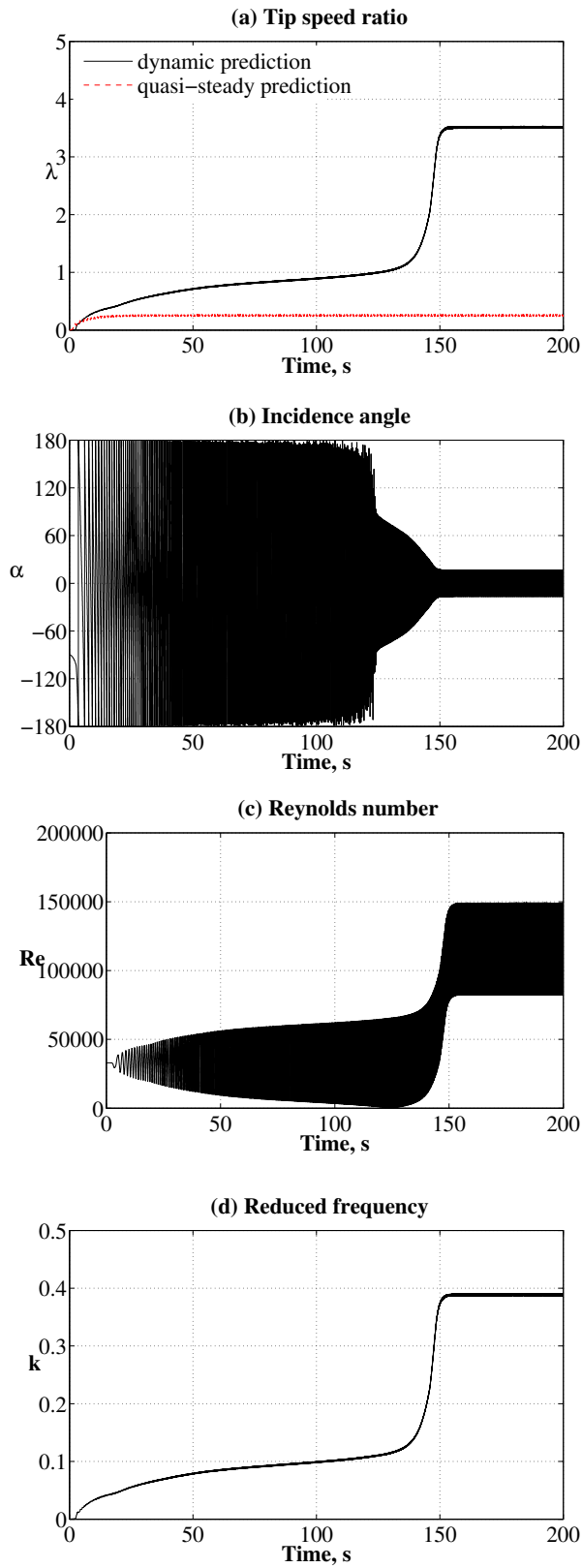
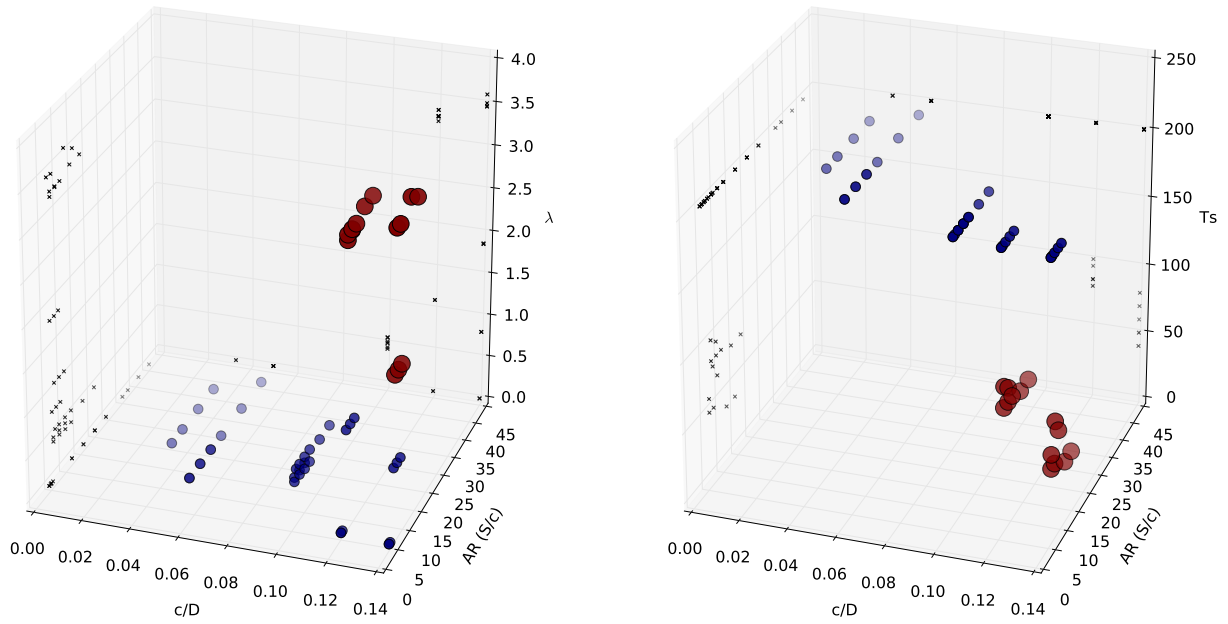Fig. 15.   DARRIEUS TURBINE STARTING BEHAVIOUR AND FLOW CONDITIONS THAT THE BLADE EXPERIENCES GTP-15-1321

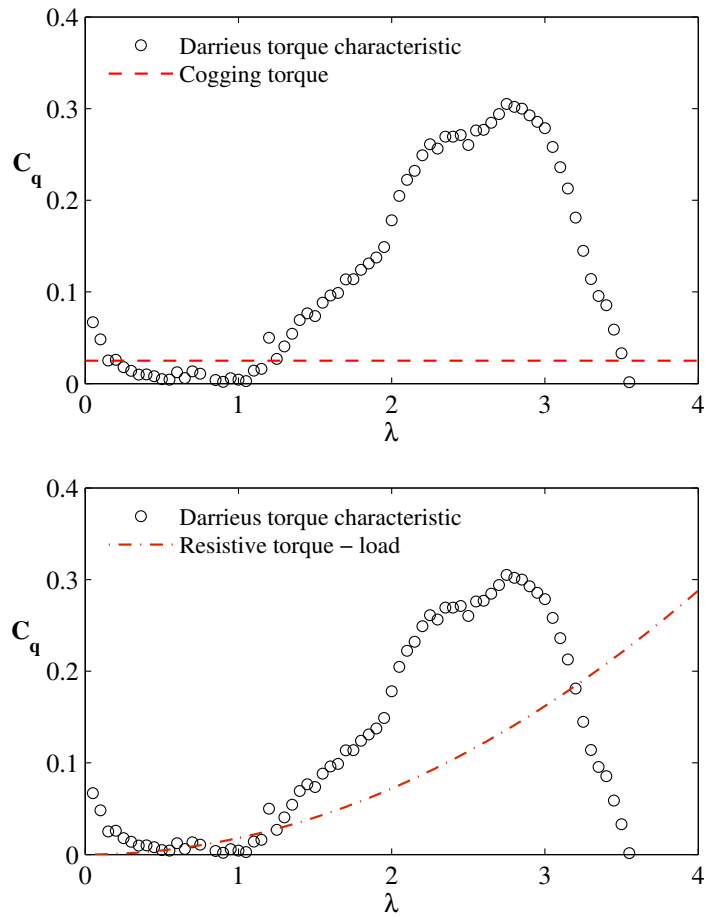Fig. 16. ROTOR GEOMETRY AND STARTING PERFORMANCE GTP-15-1321

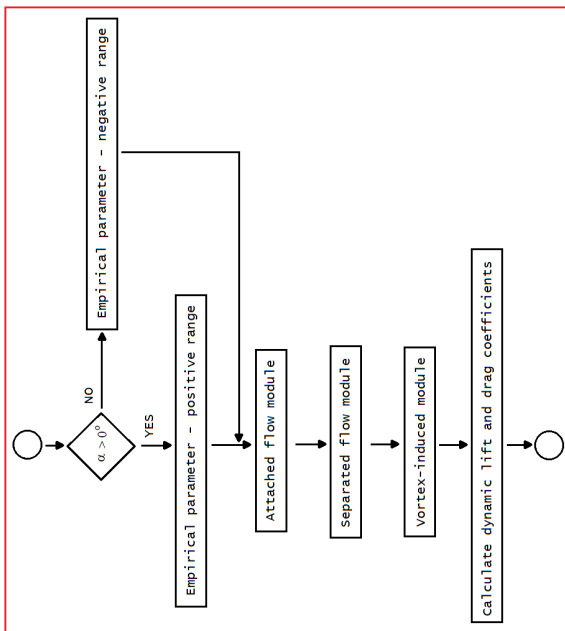

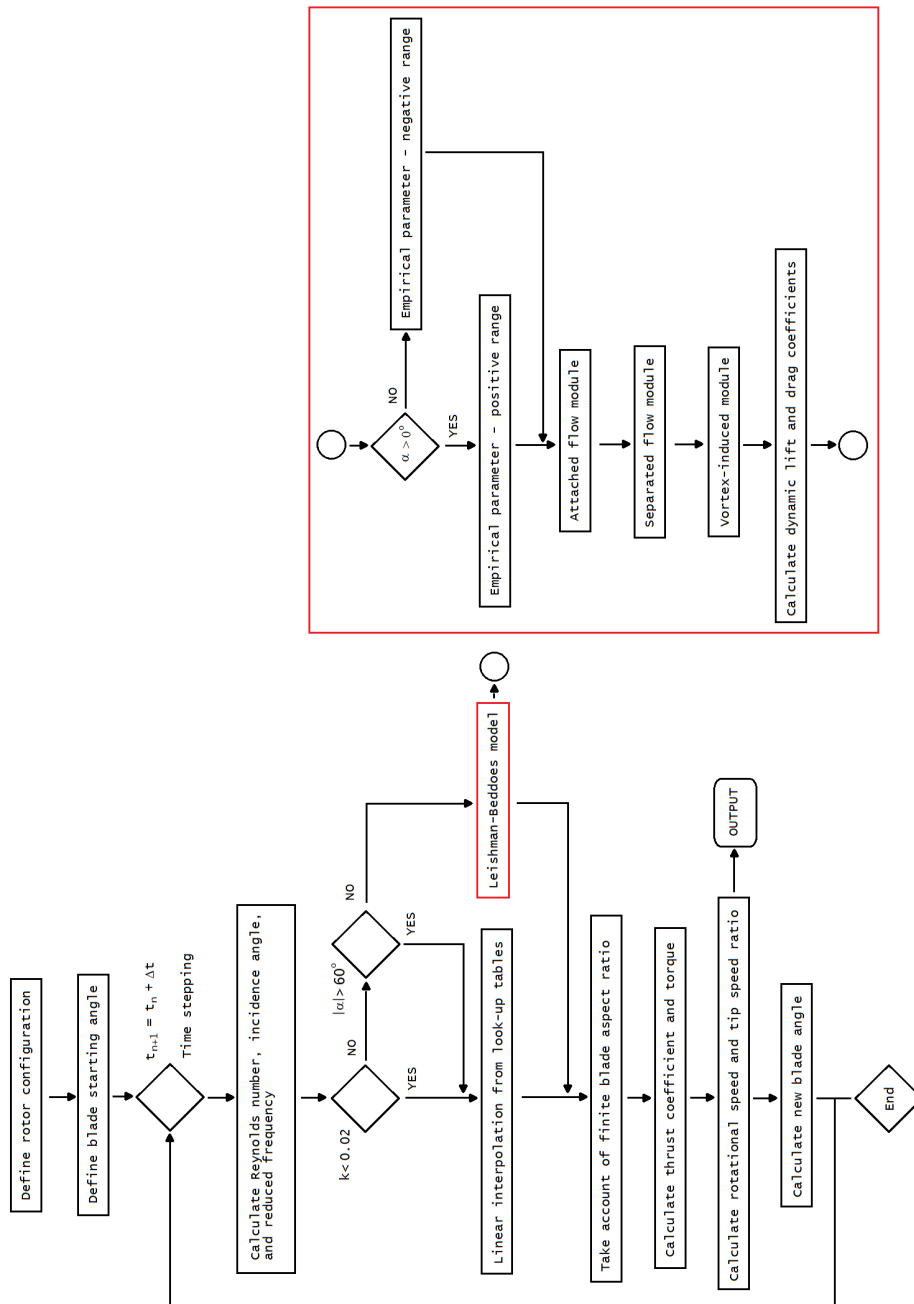Fig. 17. COGGING AND RESISTIVE TORQUES GTP-15-1321

Fig. 18.   BLOCK DIAGRAM OF STARTING BEHAVIOUR MODEL GTP-15-1321